Green Chemistry

Cutting-edge research for a greener sustainable future

Self-Cleaning Catalysts

ROYAL SOCIETY
OF **CHEMISTRY**

PAPER
Steven P. Crossley *et al.*
Self-cleaning catalysts enable recycling of multilayered plastic films

25 YEARS
ANNIVERSARY

PAPER

Check for updates

Self-cleaning catalysts enable recycling of multilayered plastic films

Dai-Phat Bui, [ID] [a] Shuheng Wang, [b] Laura A. Gomez, [a] Tahmid Ul Karim, [a] Thomas S. Salas, [a] Samira Abdolbaghi, [a] Kevin Nelson, [c] Lance L. Lobban, [a] Christos T. Maravelias [ID] [b] and Steven P. Crossley [ID] *[a]

Multilayered plastic films containing polyethylene (PE) and poly(vinyl alcohol-*co*-ethylene) (EVOH), are of great importance for the food and pharmaceutical industries. However, economical recycling is challenging for these materials, leading to waste accumulation in landfills. Mechanical recycling produces a low-value mixture of immiscible phases. Here, we describe a new approach that employs a biphasic solvent system with interfacially active catalysts to selectively remove oxygen from EVOH within multilayered plastic films to yield a single phase of compatible polymers from this complex feed mixture. This approach offers great potential for selective reactions and separation of plastic waste. An economic evaluation simulates an industrial scale recycling process for the PE product with the minimum selling price of $0.90 per kg, which is below the market price, indicating promise for the economical recycling of multilayered films.

Green foundation

1. We report here a new strategy that will enable re-use of materials and minimize the production of non-renewable byproducts through a catalytic cleanup approach.

2. Through technoeconomic analysis we reveal that this approach will enable the re-use of multilayered films to produce a recycled plastic precursor that can be sold below the current market value, which is a significant potential advancement for reducing reliance of petroleum sources in the plastic industry.

3. We currently utilize a biobased solvent to carry out the reaction (Gamma Valerolactone), which is essential to lower the energy requirements. Future iterations to improve the nature of this process would be to minimize the use of solvents. While net solvent use is minimal as reactants and products enter and exit the reactor, even the use of the green GVL solvent does require energy to heat the mixture to reaction temperature. Future efforts to explore the tradeoff associated with mass transfer *vs.* less solvent use can make the overall process greener.

1. Introduction

Multilayered plastics are not only affordable but also exhibit an excellent role in environmental barriers, making them ubiquitous in the food and pharmaceutical packaging industries. They account for a significant portion of global polymer waste.[1–3] Multilayered plastics in food packaging films commonly include a combination of polyethylene (PE) – a nonpolar polymer useful for water vapor barrier and heat sealability, and poly (vinyl alcohol-*co*-ethylene) (EVOH) – a polar polymer for the oxygen barrier.[4–7] Unfortunately, virtually none of the multilayered plastics produced are recycled due to component immiscibility, which leads to degradation of the

performance of the products.[8,9] Due to their complex nature, multilayered films are relegated to alternative end-of-life processes such as landfilling, combustion, or pyrolysis.[4–7,10] Because polyolefins constitute the largest market polymer, with a market size of 120 billion USD, this work utilizes a biphasic reaction system to carry out the selective deoxygenation of only the EVOH component of multilayered films in a single reactor at slightly above the EVOH melting temperature, facilitating the production of a single product stream that is compatible with polyolefins. This single-pot approach minimizes energy and downstream separation, which can translate to economic benefits as we will show later.

In order to carry out the desired selective deoxygenation of the EVOH component on multilayered films, TiO2 nanotubes (TNTs) are used as a catalyst support due to their external and accessible surface to carry out reactions. To favor H2 activation and create highly active interfacial sites, Pd metal is incorporated, promoting the constant site regeneration and saturation of double bonds, resulting in the formation of PE chains while

[a]School of Sustainable Chemical, Biological & Materials Engineering, University of Oklahoma, Norman, OK, USA. E-mail: stevencrossley@ou.edu
[b]Department of Chemical and Biological Engineering, Princeton University, Princeton, New Jersey, USA
[c]Amcor, Neenah Innovation Center, Neenah, WI, 54956, USA

preserving the carbon backbones of the polymer. Iron (Fe) was also incorporated to provide magnetic properties to the support, facilitating catalyst recovery and ensuring high purity of the PE products. Thus, this surface modification of TiO_2 nanotubes with Pd (Pd/TNTs) and Pd–Fe (Pd/mTNTs) exhibits a high activity and selectivity for deoxygenation of EVOH and commercial multilayered plastic films.

Biphasic reaction mixtures allow for many advantages in selective chemistry of streams of varying hydrophobic character, ranging from process intensification[11] to enhancements in rate and catalyst stability.[12–14] The use of a biphasic mixture to carry out this reaction enables the stabilization of the catalyst at the interface of the two immiscible phases, γ-valerolactone (GVL, polar) and decalin (non-polar). Conversion of EVOH to PE in a single-phase produces PE coated catalyst particles, which induce a diffusion barrier for further reaction. We hypothesize that introduction of a second phase may facilitate the continuous recovery of the product into the non-polar phase by washing it from the catalyst surface to yield a stream compatible with PE. Additionally, it eliminates the need for multiple solvents and antisolvents for plastic separation and creates a dynamic reaction system for continuous catalyst separation and product collection during the reaction. GVL was selected as the polar solvent due in part to its production from renewable biomass sources[15] as well as its ability to disperse a molten EVOH phase.[16] Decalin, the non-polar solvent, supports the migration of formed non-polar polymer and regeneration of the catalyst surface coated with PE.

2. Experimental

2.1. Materials

The chemicals were purchased from Sigma-Aldrich without further purification: γ-valerolactone (GVL, 99%), decalin (mixture of *cis* + *trans*, 99%), $Pd(NO_3)_2 \cdot 2H_2O$ (~40% Pd basis), $Fe(NO_3)_3 \cdot 9H_2O$ (99.99 trace metal basis), Poly(vinyl alcohol-*co*-ethylene) (EVOH, T_m = 180 °C, 32 mol% ethylene), paraffin wax, HNO_3, and TiO_2 (nano-powder < 25 nm, Mixture of rutile : anatase/85 : 15). The gases were purchased from Airgas: nitrogen (N_2, ultra-high purity GD 5.0) and hydrogen (H_2, ultra-high purity GR 5.0 CGA 350). The multilayered film is a commercial food packaging film provided by Amcor without further purification, with a profile as shown in Table S1.

2.2. Catalyst synthesis and characterization

TiO_2 nanotubes (TNTs) were synthesized by dispersing 1.7 g of TiO_2 in 157 mL of NaOH 10 M solution, followed by a hydrothermal process at 135 °C for 24 h. The resulting mixture was neutralized with HCl, washed several times with DI water, and dried at 60 °C. The resulting dried powder was subsequently calcined at 350 °C for 2 h.

Metal-functionalized TiO_2 nanotubes were prepared using the incipient wetness impregnation method with metal nitrates as a precursor. For magnetic-functionalized TiO_2 nanotubes (mTNTs), $Fe(NO_3)_3 \cdot 9H_2O$ was used as a precursor to obtain 5 wt% Fe_3O_4 on the TNTs. For Pd on TiO_2 nanotubes (Pd/TNTs) $Pd(NO_3)_2 \cdot 2H_2O$ was used as a Pd precursor to achieve 2 wt% Pd on the TNTs. For Pd on magnetic-functionalized TiO_2 nanotubes (Pd/mTNTs), the mTNTs were washed with paraffin wax to protect the Fe incorporated into TiO_2 nanotubes. $Pd(NO_3)_2 \cdot 2H_2O$ was then added as a Pd precursor, with a weight ratio of 2 : 5 : 100 wt% for Pd : Fe_3O_4 : TNTs. The catalysts were sonicated for 60 min, dried at 80 °C for 12 h in a vacuum oven, and then calcined at 350 °C for 2 h.

The diameter of Pd for Pd/TNTs and Pd/mTNTs were imaged by using a JEOL Grand ARM STEM, operated at 300 kV, with a high-angle annular dark-field (HAADF-STEM) detector. For elemental mapping analysis, energy-dispersive spectroscopy (EDS) was employed, with detection facilitated by a dual 100 mm^2 silicon drift detector (SDD). These samples were previously reduced at 195 °C during 30 min. The TEM/STEM sample grids were prepared by dispersing the sample in ethanol for 10 minutes, then drop-casting approximately 5 μl onto the lacy carbon film-coated copper grids using a pipette and drying under ambient conditions.

The thermogravimetric analysis – temperature-programmed reduction (TGA-TPR) was conducted using a Netzsch STA 449F1 TGA system integrated with a QMS 403 C Aeolos quadrupole mass spectrometer. The sample is a 50 mg catalyst, heated from room temperature to 195 °C with a ramping step of 2 °C min^{-1}. The signals of H_2 consumption (m/z = 2) and H_2O evolution (m/z = 18) were recorded.

Powder X-ray diffraction (XRD) was conducted on a Rigaku SmartLab X-Ray diffractometer equipped with a Cu–K-Alpha radiation source. The operating conditions were as follows: the wavelength was 1.54059 Å, the X-ray source voltage was 45 kV, the amperage was 200 mA, and the scan rate was 10θ min^{-1}. Reference peaks were obtained from materials data, incorporated MINERAL database.

2.3. Catalytic conversion of EVOH and commercial multilayered films

The deoxygenation of EVOH and commercial multilayered films over metal oxide catalysts was studied in monophasic and biphasic solvent systems. The reaction was conducted in a three-neck round-bottom flask equipped with a Graham condenser, a glass tube for gas bubbling into the solvent, and a removable glass stopper for adding chemicals. For the monophasic system, 5 mL of GVL was used as the solvent, while a mixture of 5 mL of GVL and either 10 mL of decalin or 2 g of PE was used as the biphasic system. The solvent was added into the flask while maintaining a 60 mL min^{-1} H_2 flow, and the mixture was heated to the desired temperature. At 195 °C, 10 mg of catalyst was added for a 30 min reduction. Following this, 100 mg of EVOH or commercial film was introduced into the system. After the reaction, the mixture was transferred to a 50 mL centrifuge tube and cooled by immersion in water. The product was separated from the solvent by centrifugation and washed twice with acetone. Finally, the product was dried at 60 °C for 24 hours.

The products from the reaction conducted with EVOH were dissolved in d-DMSO for NMR analysis. The non-polar and polar polymers were then separated by dissolving the non-polar polymer in decalin at 100 °C for 6 h. After washing the residual solids containing the polar polymer and catalyst twice with acetone, their weight was recorded. The non-polar polymer was separated from the decalin phase by centrifugation, washed twice with acetone, and its weight was also recorded. For NMR analysis, the polar polymer was dissolved

them with fresh decalin solvent. In the experiment conducted with multilayered packaging film in a biphasic system, decalin was replaced at different rates (no replacement, 5 mL every 30 min, 5 mL every 5 min). Prior to solvent removal and addition, stirring was ceased one minute prior to solvent extraction in order to avoid removal of any EVOH phase or catalyst. Decalin was pre-heated to 185 °C to minimize temperature drop before being injected into the reaction system. The products were then collected and analyzed as described above.

$$\text{Percent of O removed (\%)} = \frac{\Delta \text{ moles of oxygen in EVOH (mol}_O)}{\text{initial moles of oxygen in EVOH (mol}_O)} \times 100\% \tag{1}$$

$$\text{Rate of deoxygenation}(M_O\,g_{cat}^{-1}\,h^{-1}) = \frac{\Delta \text{ moles oxygen in EVOH (mol}_O)}{V_{solution}\,(L) \times \text{mass of catalyst (}g_{cat}) \times \text{reaction time (h)}} \tag{2}$$

$$\text{Rate of deoxygenation}(M_O\,g_{cat}^{-1}\,h^{-1}) = k \times C_{EVOH}{}^a \times p_{H_2}{}^b \tag{3}$$

$$\text{TOF per surface Pd metal (s}^{-1}) = \frac{\text{rate of deoxygenation }(M_O\,g_{cat}^{-1}\,h^{-1}) \times V_{solution}\,(L) \times M_{Pd}(g_{Pd}\,mol_{Pd}{}^{-1})}{w\%_{Pd}(g_{Pd}\,g_{cat}{}^{-1}) \times D\%\left(\frac{Pd\,site_{surface}}{Pd\,site_{total}}\right) \times 3600\,(s\,h^{-1})} \tag{4}$$

$$\text{TOF per bulk Pd metal (s}^{-1}) = \frac{\text{rate of deoxygenation}(M_O\,g_{cat}^{-1}\,h^{-1}) \times V_{solution}\,(L) \times M_{Pd}(g_{Pd}\,mol_{Pd}{}^{-1})}{w\%_{Pd}(g_{Pd}\,g_{cat}{}^{-1}) \times 3600\,(s\,h^{-1})} \tag{5}$$

in d-DMSO at 80 °C for 12 h, while the non-polar polymer was dissolved in d-CDCl₃ at 40 °C for 24 h. For this analysis, a 400 MHz Varian VNMRS NMR spectrometer was used for ^{1}H NMR analysis. Prior to each run, the procedure included shimming, locking the z_0 position, and autotuning. The number of scans was set to 16, and the block size was set to 4. The kinetics of the deoxygenation of EVOH over the catalysts were studied to explore the mechanism.

The percentage of oxygen removed was calculated by eqn (1). The initial rates were calculated by extrapolating all reaction rates (eqn (2)) to the reaction time of 0 h. Initial rates (mol g_{cat}^{-1} h^{-1}) for various EVOH concentrations (mol L^{-1}) and partial pressures of H_2 (atm) were used to obtain the reaction order (eqn (3)). The turnover frequency (TOF) (eqn (4) and (5)) was calculated using the deoxygenation rate, Pd weight percentage content (w% Pd), and metal dispersion, with dispersion values derived from CO chemisorption. CO chemisorption data for Pd/TNTs are reported in our recent publication.[17]

2.4. Intermittent organic phase replacement

The organic phase was intermittently replaced by removing the non-polar products in fixed time increments and replacing

2.5. Techno-economic analysis for plastic upcycling in a biphasic system

The mass balance parameters for the reactor and all parameters associated with the flash drum and distillation column were estimated from simulations in Aspen V14. Parameters governing reaction kinetics and conditions were taken from experiment results, while other parameters (energy consumption, costs, sizing rules of thumb, etc.) were taken from literature. We used optimization methods to simulate a facility using the proposed large-scale multilayer film recycling process and determine the minimum selling price (MSP) of the recycled LDPE product. The MSP is the price at which the final product must be sold to offset the total production cost, that is, the price needed to achieve a net present value (NPV) of $0. The NPV accounts for capital investment costs, discounted cash flows (income, costs, depreciation) throughout the facility's lifetime, as well as any salvage value remaining at the end of the facility lifetime. The MSP is a commonly used metric which allows us to compare the economic viability of different processes by finding the lowest product price which does not result in financial loss. The objective of the model was to find the MSP of the recycled LDPE product on a per-

kilogram basis, given a feed basis of 375 kg h^{-1} and constraining the NPV to be \$0. The optimization model was formulated in GAMS (42.5.0). Each process unit had its own cost, utility needs, and mass balance parameters. Our model contained 536 constraints and 421 variables, covering mass balances, unit specific considerations, sizing calculations, energy balances, and economic calculations. In total, our modelled process contained 22 streams. For a detailed process flow diagram, see Fig. 1 and Table S9. The reactor operated at 1.5 atm, and all other units operated at 1 atm. See Sections S3 and S4 in the SI for detailed descriptions of each process unit.

The amount of GVL and decalin used in the process was adjusted to achieve a concentration of 33.3 kg m^{-3} for film components in the liquid phase of the reactor. Hydrogen gas was provided in excess, with H$_2$ partial pressure maintained above 0.5 atm to prevent unwanted side products. The reactor was sized to give a gas residence time of at least 2 min and a liquid residence time of 1 hour. The catalyst loading in the reactor was set to 10 wt% of the hourly film feed flow, resulting in 37.5 kg of catalyst for a 375 kg h^{-1} feed flow.

In the experiments, we demonstrated that a layer of LDPE and decalin naturally forms at the top of the reactor and can be continuously removed to maximize deoxygenation rates. To model this process, a continuously stirred tank reactor (CSTR) was used for the reaction, followed by a decanter phase separation. The liquid stream from the CSTR was sent to the decanter, where GVL, trace water, and catalyst were recycled back to the CSTR. The LDPE and decalin (the top phase of the decanter) were sent to a cooling tank to be cooled to 40 °C, causing LDPE to solidify. This mixture was sent to a vacuum rotary drum filter, which produced filter cake with 40 wt% decalin, with the remaining decalin being recycled back to the reactor. The filter cake was then sent to a rotary dryer to remove any

remaining decalin, which was condensed and recycled back to the reactor. Finally, the dried LDPE was sent to an extruder to produce pellets for sale.

Excess unreacted H$_2$ gas, water vapor, and evaporated solvent from the CSTR were sent to a flash drum. In the flash drum, all H$_2$ gas and some of the water vapor were purged to prevent excessive water build-up in the reactor. The liquid stream from the flash drum was then sent to a distillation column to remove the remaining water. The column bottoms, containing solvent and trace water, were recycled back to the reactor, while the distillate, containing water and trace decalin, was purged. While there was some accumulation of water in the reactor, we assumed it had no impact on the kinetics of the reaction due to its low concentration. The particle size of the Pd/TNTs catalyst was estimated by measuring 100 particles.

3. Results and discussion

3.1. Selective conversion of EVOH in monophasic and biphasic reaction systems

Deoxygenation of EVOH using promoted metal oxide catalyst supports (TiO$_2$ and TNTs) was studied in monophasic and biphasic reaction systems (Fig. 2). The EVOH grades vary by ethylene content, in this work, the functional group composition of EVOH includes methyl groups (R–CH$_3$) at 0.37%, methylene groups (–CH$_2$–) at 65.84%, hydroxyl groups (–CH(OH)–) at 33.66%, and others (ethers & ketones) at 0.13%. The trace amount of ethers and ketones is from the unsaponified vinyl acetate since EVOH is produced *via* the saponification of vinyl acetate. Under reaction conditions at the temperature of 195 °C, which is slightly higher than the EVOH melting temperature but much lower than the pyrolysis temperature, EVOH exhibits excellent stability in a reducing environment in both
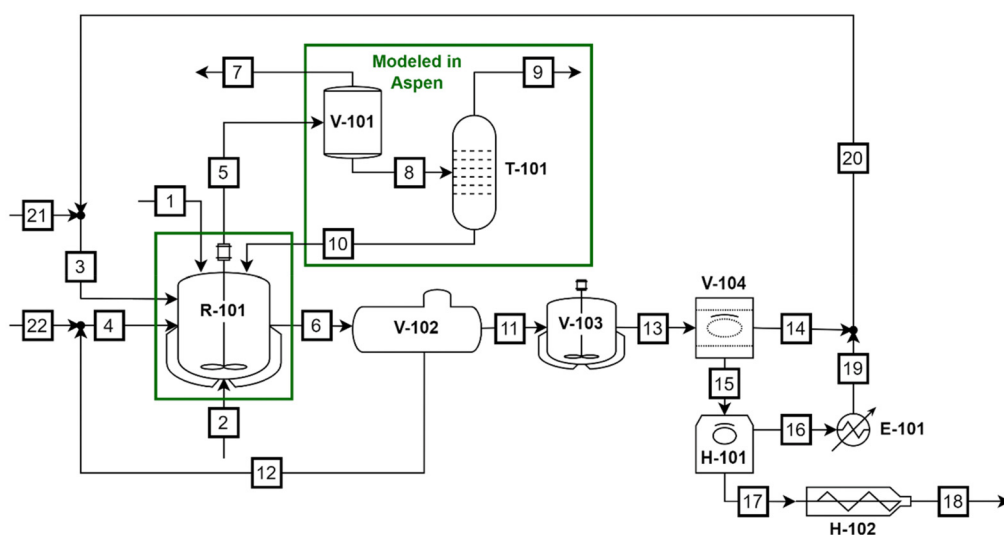

Fig. 1 Detailed process flow diagram used to generate TEA (with accompanying stream information in Table S9). Abbreviations – R-101: reactor; V-101: flash drum; T-101: distillation column; V-102: decanter; V-103: cooling tank; V-104: vacuum rotary drum filter; H-101: rotary dryer; H-102: screw extruder; E-101: condenser.
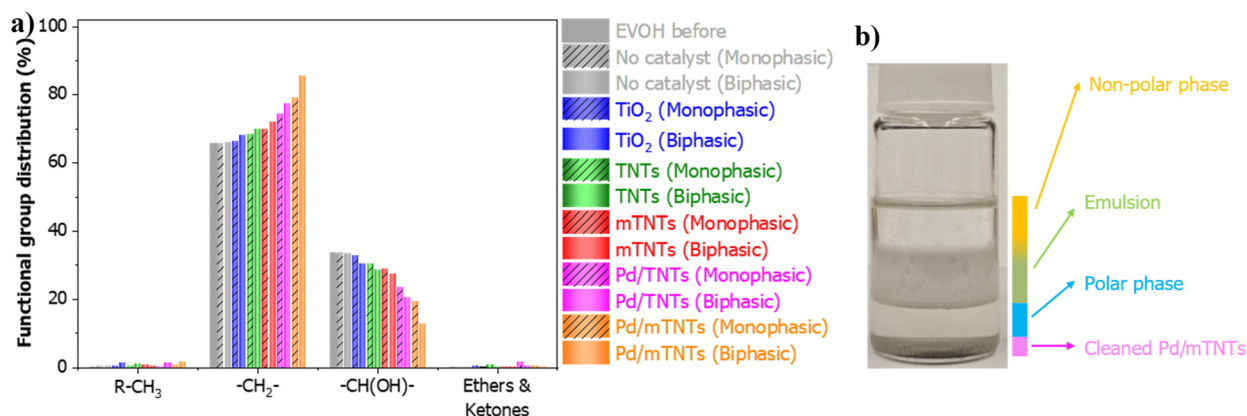
Fig. 2 EVOH conversion in monophasic *vs.* biphasic reaction systems. (a) Functional group distribution of EVOH after the reaction in monophasic and biphasic systems. (b) Schematic product fractions after reaction. Reaction conditions: $m_{catalyst}$ = 10 mg, m_{EVOH} = 100 mg, F_{H_2} = 60 mL min^{-1}, P_{total} = 1 atm, $T_{reaction}$ = 195 °C, and t_{rxn} = 1 h. For the monophasic reaction, 5 mL of GVL was used; for the biphasic reaction, 5 mL of GVL and 10 mL of decalin were employed.

monophasic and biphasic systems without the presence of a catalyst. In the presence of TiO$_2$ and TNTs, minimal dehydration rates were observed in both reaction systems. In contrast, by adding Pd and Fe metal promoters, deoxygenation rates of EVOH are greatly enhanced. These highly reactive metal–support interface sites promote enhanced deoxygenation rates while the metals also promote further hydrogenation of reaction intermediates, resulting in significant oxygen removal even in a monophasic reaction system (Fig. S1a). Reactions in a monophasic system carried out with mTNTs, Pd/TNTs, and Pd/mTNTs result in a reduction of the hydroxyl group content of EVOH to 28.8%, 23.7%, and 19.4%, respectively. This is in line with our previous studies on the deoxygenation of EVOH over acid sites alone and upon incorporation of metals.[16,18]

Notably, the deoxygenation rates of EVOH over Pd/mTNTs differ significantly between monophasic and biphasic systems. The higher activity observed in the biphasic system can be attributed to enhanced removal of accumulated polymer films from the catalyst surface. This second phase facilitates the migration of non-polar products, which have less than 19.4% hydroxyl groups (~42.5% of O removed), to the non-polar solvent, thereby promoting further conversion of EVOH. By replacing decalin with PE as the non-polar phase of the biphasic reaction system, a system resembling industrial process conditions was utilized to assess the capability of the biphasic systems, where the solvent usage is minimized and the products are maximized. The deoxygenation over Pd/mTNTs is still better than in a monophasic solvent system (Fig. S1b). It is also noteworthy that the levels of methyl groups and ethers/ketones did not increase substantially (Fig. 2), suggesting that deoxygenation is the predominant reaction occurring over these catalysts. Thus, the addition of metal promoters facilitates the deoxygenation of the EVOH while minimizing the cleavage of C–C bonds.

As illustrated schematically in Fig. 3, the polar phase (GVL) dissolves EVOH and contains the catalysts, enabling inter-
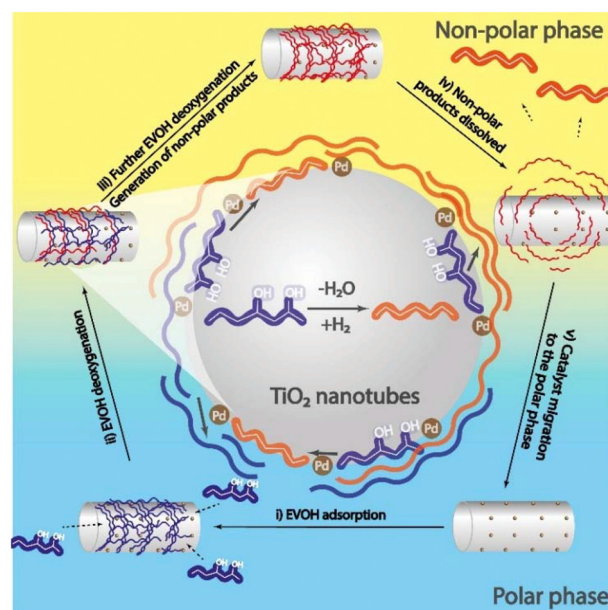

Fig. 3 Schematic illustration of the deoxygenation of EVOH occurring at the GVL/decalin interface in the solid-stabilized emulsion.

action between EVOH and the catalyst surface. As the reaction proceeds, the catalyst becomes coated with non-polar products, decreasing its density and dispersibility in the polar solvent. These coated catalysts migrate to the interface between the two phases, forming an emulsion. The non-polar converted catalyst then migrates to the non-polar solvent, cleaning the catalyst surface and preventing further conversion. In contrast, EVOH-containing polymer remains in the GVL phase and continuously reacts when in contact with fresh catalyst. This result illustrates the concept of simultaneous reaction and further separation of new formed compounds, which are now chemically identical to polyethylene.

Additionally, the magnetic properties of the catalysts, Pd/mTNTs, can be used to enhance the effective separation and recovery of the catalyst.

To gain insight into the mechanism of the deoxygenation of EVOH polymers, the moles of EVOH and partial pressure of H_2 were varied, as depicted in Fig. 4. The corresponding reaction rates are provided in Fig. S2. Our findings reveal a linear relationship between the deoxygenation rate and the initial amount of EVOH, indicating that the deoxygenation rate is first-order with respect to EVOH for all tested catalysts (Fig. 4a). This suggests that the catalyst surface is not fully covered by EVOH. For TiO_2 and TNTs, the reaction order with respect to H_2 is approximately zero, as expected, indicating that H_2 is not kinetically relevant during the dehydration of EVOH over the acid sites present on TiO_2. However, with the incorporation of metal promoters (Pd or Fe), the reaction order with respect to H_2 interestingly becomes negative for mTNTs, Pd/TNTs, and Pd/mTNTs (Fig. 4b). The incorporation of Pd and Fe promotes the formation of defects or oxygen vacancies (Ti^{3+} cations) on the TiO_2 surface, significantly boosting deoxygenation rates. Our previous works have demonstrated that the sites located at the metal–support interface are primarily responsible for most of the selective deoxygenation of alcohols and aldehydes over Pd/TiO$_2$.[19–21] Here, we hypothesize that a hydroxyl group from EVOH binds to an oxygen vacancy near

the interface and weakens the C–OH bond to facilitate selective cleavage. This H removal step before C–OH bond breaking can explain the half-order negative dependence with respect to H_2 observed experimentally. Negative hydrogenolysis rate dependencies with respect to hydrogen partial pressure are well established.[22,23] This is explained by the required formation of bonds between the carbon on the molecule and the catalyst surface prior to the kinetically relevant C–O cleavage step, and a hydrogen removal step must accompany the formation of this new metal–carbon bond. Further, this inverse dependence with respect to hydrogen provides evidence that the reaction is not limited by flux of H_2 to the catalyst surface, which would exhibit positive first order behavior.

Fig. 4c describes the two competing parallel pathways that can occur over Pd/TNTs or Pd/mTNTs. One pathway involves selective deoxygenation at the interface between the metal and the support, where undercoordinated centers at the metal support interface promote weakening of the C–O bond, resulting in the formation of deoxygenated compounds.[19,21,24] The other possible pathway takes place on acid sites present on the TiO_2 surface,[25,26] where EOVH dehydration occurs. This results in the formation of alkenes that can be further hydrogenated over metal sites to yield the same deoxygenated products. If deoxygenation occurs *via* a kinetically relevant dehydration pathway over acid sites, followed by rapid hydrogenation of unsaturated
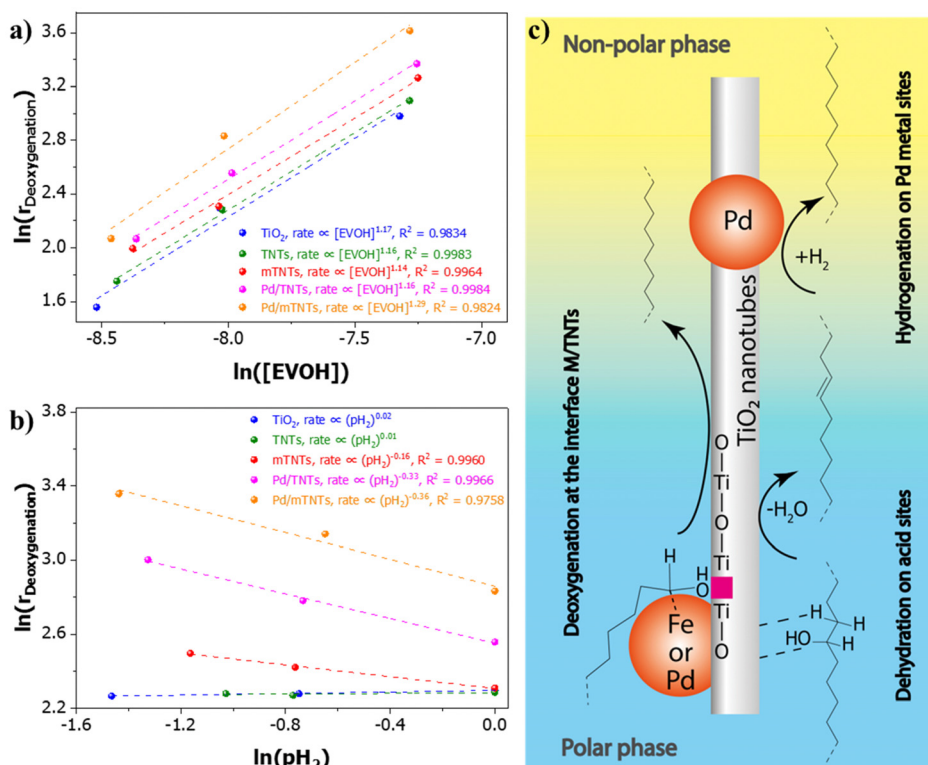

Fig. 4 Deoxygenation of EVOH over TiO_2 nanotubes catalyst supports. (a) Initial deoxygenation rate *vs.* OH concentration and (b) H_2 partial pressure and (c) proposed pathway for deoxygenation of EVOH over the Pd/mTNTs catalyst. Reaction conditions: (a) m_{EVOH} = 30 mg, 50 mg and 100 mg with P_{H_2} = 1 atm (b) P_{H_2} = 0.2, 0.5 and 1 atm with m_{EVOH} = 50 mg. For all the reactions: $m_{catalyst}$ = 10 mg, F_{total} = 60 mL min^{-1}, $T_{reaction}$ = 195 °C and initial rates of deoxygenation at 0 min are extrapolated from the reaction rates at 5 min, 10 min, and 15 min.

products on the metal, a 0th order hydrogen dependency will result. Thus, the reaction orders observed ranging from −0.36 to 0th order represent the relative kinetic importance of a C–O hydrogenolysis path (which we presume is −0.5 order with respect to H_2) *vs.* a dehydration path (0th order).

Small increases in intermediate side products become observable at the lowest tested hydrogen pressures (∼2.5 PSIA), (Fig. S3). Under these conditions, the lower hydrogen pressure leads to an enhancement in acid catalyzed isomerization reactions as illustrated in Fig. S4, amounting to ∼1% or less of the functional group distribution. Given sufficient time and a metal function, these ketones can be deoxygenated to form the same polyethylene-like compounds discussed previously.[27,28]

EDS-STEM analysis in Fig. S5 and S6 indicates that Fe and Pd are dispersed over the TiO_2 nanotubes, with some small agglomerations of Pd atoms. Based on STEM analysis, Pd particle size distribution for Pd/TiO_2 is 0.6 to 1.2 nm, as shown in Fig. S7 and S9a. These results are consistent with previous CO chemisorption analysis of this sample.[17] The addition of Fe to Pd/TNTs, intended to add magnetic properties, leads to an increase in the overall metal particle size, as observed in STEM images (Fig. S8). The particle size distribution, based on STEM analysis, indicates a size range of 2–3 nm, as shown in Fig. S9b. The incorporation of Pd onto TNT drastically increases the number of Ti^{3+} at the surface.[17] TPR-TGA results for Pd/mTNTs show a slightly greater mass loss (0.62 wt%) than Pd/TNTs at the reaction temperature (Fig. S9c), suggesting that the incorporation of Fe onto the Pd/TNTs catalyst slightly enhances its reduction behavior, and as a consequence increasing Ti^{3+} sites. However, for Pd/mTNTs, accurately estimating particle size from STEM or CO chemisorption is challenging due to the formation of isolated Fe and Pd clusters as well as Pd–Fe alloy clusters. Fig. S10 presents the turnover frequency results based on Pd surface metal sites and per bulk Pd metal. These results suggest that incorporating Fe not only provides magnetic properties but also enhances the overall activity when normalized to the number of bulk Pd atoms.

3.2. Catalytic conversion of multilayered films to polyethylene in a single pot

To evaluate the effectiveness of the catalysts in more practically realistic applications, we conducted deoxygenation reactions on commercial multilayered films. These raw plastic films contain 20 wt% of polar EVOH polymer and 80 wt% of non-polar low-density polyethylene (LDPE) and tie layer polymers; further details about their components can be found in Table S1. Post-reaction, the weights of both non-polar and polar polymer fractions were obtained, with the reactions performed in a biphasic system. Notably, the reaction could not be carried out in a monophasic system using only GVL or decalin, as these solvents did not fully dissolve the multilayered films. In the absence of a catalyst, no thermal polymer degradation or other side reactions were observed under reaction conditions, as indicated in Fig. 5a and further confirmed by NMR results in Fig. S11, which also confirms solvent stability during the catalytic reaction. In addition, we have monitored the loss in liquid sample before and after reaction and noted that during this time no significant GVL liquid sample losses were detected. We note that some reports have observed some ring opening and closing under similar conditions in the presence of more active acid catalysts at higher temperatures.[29] While we cannot rule out the possibility of reversible ring opening and closing *in situ* during our reaction conditions, GVL does not appear to experience any significant net conversion under the reaction conditions and catalyst system we report here. Our results indicate that the deoxygenation of the pure EVOH over the catalysts is highly comparable to that of commercial film, even in the presence of PE and tie layer content. We hypothesize that as the multilayered films dissolve, PE preferentially migrates to the non-polar phase, thereby not impacting the rate of deoxygenation of the EVOH in the commercial film. Here, TiO_2 and TNTs show negligible deoxygenation rates, as shown in Fig. 5a. However, deoxygenation rates increase with the use of promoted metal oxides, mTNTs, Pd/TNTs, and Pd/mTNTs, resulting in a higher production of PE products. This promising approach highlights the potential of these catalysts for upcycling of multilayered films.

To simulate the continuous deoxygenation of the plastic waste to better mimic a continuous industrial process, the non-polar products were intermittently removed from the system by replacing with fresh organic solvent or using desired products as a non-polar phase (Fig. 5b). The replacement of non-polar solvents in the biphasic system decreases the PE concentration that accumulates in that phase, promoting further extraction and separation of deoxygenated EVOH products from the catalyst surface. With a decalin replacement rate of 50% of the decalin solvent every 30 min (5 mL per 30 min), a slight increase in deoxygenation was observed for the commercial film over Pd/mTNTs. However, with a faster replacement rate of 5 mL every 5 min, deoxygenation drastically increased, resulting in nearly 100% oxygen removal from commercial multilayered films over the same time frame. By employing a biphasic system of GVL as polar phase and PE as non-polar phase without any replacement during the reaction, the deoxygenation remained excellent, with nearly 100% oxygen removal. This can be attributed to non-polar phase PE, which is highly compatible with the products, allowing it to better attract these products right after the small cluster is formed.

To demonstrate the stability of the process, deoxygenation was conducted in GVL : PE biphasic system with increasing commercial film loadings across separate experiments for simplicity. The initial commercial film mass was around 200 mg for the 1-hour reaction, and this was incrementally increased up to 1200 mg in the 6-hour reaction without replacing the non-polar phase during the runs (Fig. 5c). Remarkably, nearly 100% oxygen removal was achieved within 1 hour, even when the amount of commercial film was doubled. However, further increase of commercial film loading to 400 mg decreases the deoxygenation conversion to approximately 75%. Notably, the process maintained stable performance over reaction conducted up to 4 hours. In contrast, oxygen removal declined to 44% in
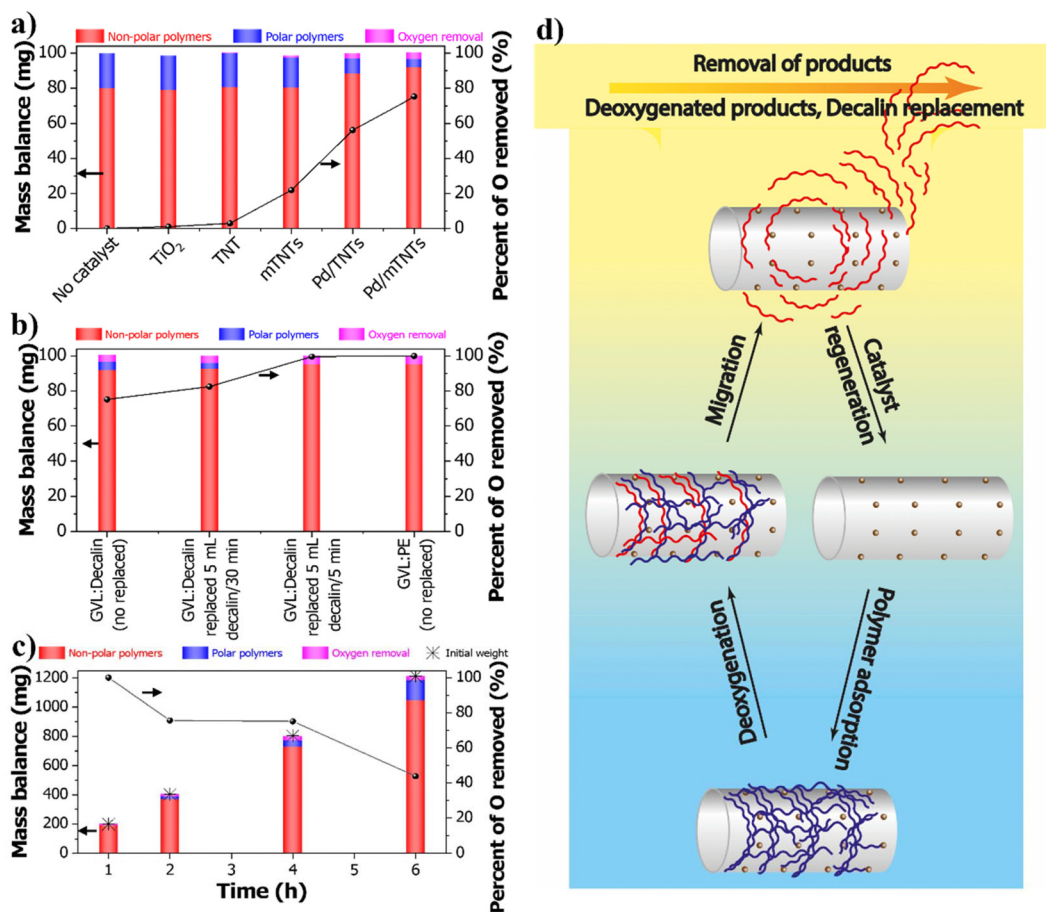
Fig. 5 Catalytic conversion of commercial multilayered film in a biphasic system. (a) Mass balance of polar and non-polar polymer after deoxygenation over different tested catalysts carried out in single-pot system. (b) Mass balance after deoxygenation over Pd/mTNTs with decalin replacement. (c) Mass balance after deoxygenation with stepwise commercial film addition over 10 mg of Pd/mTNTs in GVL : PE. (d) Schematic illustrating product removal *via* decalin replacement. Reaction condition: $m_{catalyst}$ = 10 mg, F_{H_2} = 60 mL min^{-1}, P_{total} = 1 atm, $T_{reaction}$ = 195 °C and $t_{reaction}$ = 1 h. A biphasic system composed of 5 mL of GVL and either 10 mL of decalin or 2 g of PE was used.

the 6-hour reaction, likely due to excess accumulation of EVOH to the point where it created a barrier over the catalyst that limits hydrogen diffusion to active sites, which could be corrected in a continuous process by utilizing the magnetic properties of the catalyst to retain it in the GVL phase or decreasing the rate of EVOH to catalyst introduction. In a truly continuous process, one would separate the catalyst from the PE phase by utilization of the magnetic properties of the catalyst to retain it in the GVL phase, which we anticipate would extend catalyst lifetimes even further than what is observed here. A schematic depicting the ideal process is shown in Fig. 5d.

To demonstrate the stability of the catalysts, the XRD patterns of Pd/TNTs and Pd/mTNTs at the beginning, after reduction, and after reaction are recorded as shown in Fig. S12. The results show that the predominant crystal structures of these functionalized TNTs are anatase TiO$_2$, with smaller secondary peaks of rutile TiO$_2$. There are no visible peaks for Fe and Pd on TNTs at the beginning, after reduction, or after reaction. This is consistent with the metal particle size measurements obtained through STEM, and shows that, if

Ostwald ripening is occurring, the metal crystal size stays below the detectable limits of the XRD instrument. There is a broad peak in the Pd/mTNTs at 2θ of 34 degrees, which disappears after reduction and after reaction. This peak most likely corresponds to the (104) plane of α-Fe$_2$O$_3$ (Hematite), which disappears when the hermatite is partially reduced. A comparison of the XRD references for Fe and possible iron oxides of the Pd/mTNTs are shown in Fig. S12b. While the reduction conditions should not be sufficient to reduce hematite to magnetite or Fe it is possible that the Pd metals facilitate the reduction of the iron oxides,[30] causing the XRD pattern to be disrupted. There are additional broad peaks at 2θ of approximately 28 and 49 degrees in the Pd/mTNTs after reaction. This could be ascribed to the formation of hydrated TiO$_2$ resulting from the interaction between H$_2$O and rutile TiO$_2$ (110) surface,[31,32] the formation of magnetite, the formation of Fe(OH)$_2$,[33] or even the accumulation of turbostratic carbon.[34] It should be noted that the presence of magnetite is expected to produce a stronger (311) peak at around 2θ of 35 degrees. Further characterization would be necessary to more

definitively identify this feature, but it is clearly only apparent in the Fe containing samples. The absence of chemical decomposition or detectable metal particle signals in the catalysts following the reaction indicates their stability in the process.

3.3. Techno-economic analysis of plastic upcycling using a biphasic reaction model

To evaluate the potential of using the described catalytic reaction to recycle multilayer films at scale, we simulated a recycling process utilizing the biphasic catalytic system. This process includes a reactor where the catalytic reaction converts EVOH to LDPE and downstream separation and processing units necessary to produce a final recycled pellet suitable for sale. This analysis will lead to a more accurate assessment for recycling multilayer films on an industrial scale.[35]

Fig. 6a shows a simplified flowsheet for the proposed process. The feed stream is 375 kg h^{-1} of plastic film with an 80 wt% LDPE and 20 wt% EVOH composition, matching the raw commercial films (Table S1). The catalytic reaction uses a Pd/mTNTs catalyst, which has the best performance based on our above results. The reactor subsystem is modeled by two key units: the reactor for the catalytic conversion and the decanter for phase separation, reflecting the biphasic experiments. The LDPE product from the reactor passes through solvent removal units (filter and dryer) before being sent to the extruder. Additional separation units, including a flash drum

and column, are used to recover solvents and purge water from the reactor's vapor outlet streams.

We built a model that integrates all mass and energy balances and cost calculations for a facility that runs the proposed process. The detailed mathematical formulation of the model can be found in the SI (Sections S3–S5). The costs include capital expenditure (CAPEX) and operating expenses (OPEX). Our CAPEX calculations account for the inside-battery-limit equipment costs (ISBL), which account for the additional costs of installing the equipment (e.g. pipes, infrastructure, shipping costs) on top of the cost of the equipment itself; outside-battery-limit equipment costs (OSBL) covering offsite costs (e.g. utility infrastructure, fencing, offices, employee amenities); engineering costs, which are associated with generating and implementing detailed designs of equipment/structure; contingency costs, to account for any unexpected costs and events; and costs of the materials (mostly solvent) needed to startup the process. The OPEX includes both a fixed portion (e.g. salaries, insurance, overhead, etc.) and variable expenses (e.g. steam and cooling water consumption, electricity usage, cost of solvents, etc.). A preliminary techno-economic analysis was conducted to determine the MSP for the recycled LDPE product.

Given the assumptions about our process, which does not include any pre-processing (e.g., cleaning) or post-processing (e.g., addition of stabilizers) steps, the calculated MSP of the final recycled LDPE product is $0.90 per kg. This MSP is lower than the current market price of virgin film-grade LDPE,
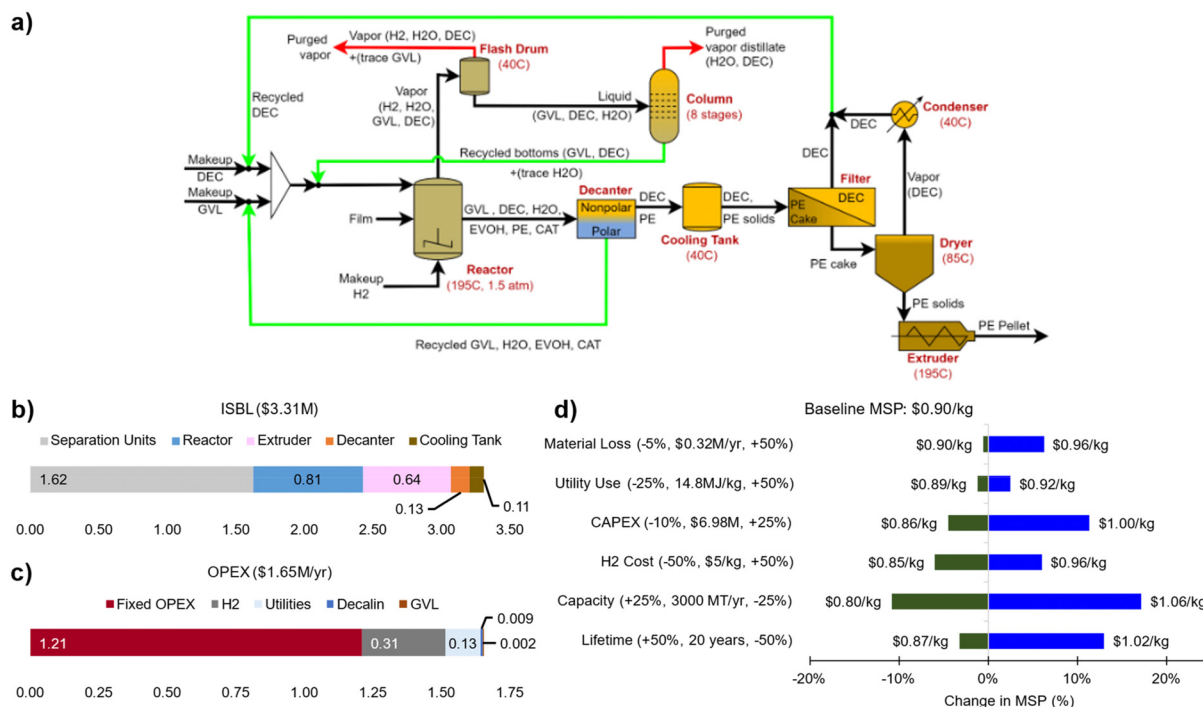

Fig. 6 Techno-economic analysis of proposed plastic upcycling process. (a) Flowsheet of the film recycling process. Abbreviations – DEC: decalin, GVL: γ-valerolactone, H2: H$_2$ gas, H$_2$O: water. (b) Unit contributions to the inside-battery-limit cost (ISBL). (c) Cost breakdown of the total operating cost (OPEX). (d) Sensitivity analysis on the MSP with respect to material loss (cost of replenishing purged/lost material), utility use (energy needed per kg of plastic recycled), CAPEX, H$_2$ raw material cost, capacity (of the facility), and lifetime (of the facility), with the range of parameter values given as (%favorable change, baseline, %unfavorable change).

which was $1.25 per kg as of March 2024 (in January 2024 dollars),[36] and is comparable to the market price of recycled, non-food grade LDPE, which stood at $0.90 per kg as of July 2023 (in January 2024 dollars).[37] A study of a dissolution–precipitation process, another promising research direction for multilayer plastic film recycling, reports an MSP of $1.62 per kg.[38] However, note that the dissolution–precipitation process can recycle multilayer plastic film with 5 materials, while our process currently recycles multilayer plastic film with two materials (EVOH and LDPE). In principle, the main advantage of our process compared to dissolution–precipitation processes is its potential to use fewer solvents and, consequently, fewer pieces of equipment, as we do not need to selectively dissolve and precipitate each different component of the film with different solvents. Our big-picture goal is to achieve a 'one-pot' reaction which can convert all the different plastic film layer materials into pure LDPE. The current process consumes 14.8 MJ kg^{-1} of film recycled, which is ~54% less energy than the 32.1 MJ kg^{-1} needed to produce virgin LDPE.[39] These energy savings are comparable to those of existing demonstration-scale dissolution–precipitation plastic packaging recycling plants, which can lead to an estimated 40% energy savings compared to virgin PE production.[40] Note that dissolution–precipitation recycling processes have been the focus of recent research into multilayer plastic film recycling.[41] This preliminary analysis suggests that the process has the potential to be economically viable in the current market. A necessary next step would be to verify the degree of branching (and other properties) of the product to confirm that it meets the qualifications to be sold as LDPE.

Our results show that the biggest contributors to the CAPEX are the separation units, within which the filter and dryer are the major cost contributors. Fig. 6b provides a breakdown of the ISBL equipment cost of the major equipment categories, while Fig. S15a offers a more detailed breakdown of the ISBL costs of the separation unit. An important contribution to the variable OPEX is the hydrogen needed for the process. This is detailed in Fig. 6c, which breaks down the operating costs, and Fig. S15b for a further breakdown of utility costs.

A sensitivity analysis (Fig. 6d) was also conducted to examine the impacts of uncertainty in the calculated OPEX and CAPEX, facility lifetime, and facility capacity on the MSP. When investigating the impact of higher OPEX—caused by either higher cost of replenishing material lost in the process (both solvent and H$_2$) or higher utility usage—and higher CAPEX, we see that even if these costs are significantly higher, the MSP remains below the market price of virgin LDPE. The cost of H$_2$ specifically is a large economic driver because some of it is purged and must be replenished. This cost may be reduced by implementing H$_2$ recycling steps (though this may incur additional separation costs).

4. Conclusions

We demonstrate the selective deoxygenation of commercial multilayered films to PE on Pd over TiO$_2$ nanotubes, highlighting the efficiency of continuous PE removal from the GVL phase. This process utilizes decalin as a secondary solvent to dissolve the PE while simultaneously regenerating the catalyst surface. A preliminary economic evaluation of this process indicates that the minimum selling price of the produced PE is close to the current market price, at $0.90 per kg. Importantly, recycling hydrogen and reducing separation costs by eliminating the use of decalin can lead to further production improvements. Sensitivity analysis reveals several pathways to improve the economic viability of this process, making it a promising candidate for further study.

Future studies could focus on decreasing solvent usage in the process. As decalin serves purely to reduce viscosity of the non-polar phase in the reactor, it is reasonable to envision a process that does not use non-polar solvent and thus eliminates a large portion of the costs associated with non-polar solvent separation (including costs of the filter and dryer). Even without implementing these adjustments, the process becomes more economically viable if the facility lifetime is extended to 30 years, or if the facility capacity is increased by 25%. The findings reported here for polyols will likely extend to other important plastic impurities in multicomponent films, including PVC and PET, food waste, dyes, and other impurities, which will be the focus of future studies. Thus, our approach provides an economically viable solution for the continuous and direct production of pure polyethylene from plastic waste using a biphasic system.

Author contributions

D-PB: conceptualization, investigation, methodology, validation, visualization, writing – original draft, SW: formal analysis, methodology, validation, visualization, writing – original draft, LAG: methodology, validation, visualization, writing – original draft, TUK: validation, writing – review & editing, TSS: validation, writing – review & editing, SA: validation, writing – review & editing, KN: resources, writing – review & editing, LLL: conceptualization, supervision, project administration, writing – review & editing, CTM: conceptualization, software, supervision, project administration, writing – review & editing, SPC: conceptualization, resources, supervision, project administration, funding acquisition, writing – review & editing.

Conflicts of interest

There are no conflicts to declare.

Data availability

The article and SI include all relevant data and information that support this research.

Supplementary information is available. See DOI: https://doi.org/10.1039/d5gc02739j.

Acknowledgements

References

1 M. Zare, P. A. Kots, S. Caratzoulas and D. G. Vlachos, *Chem. Sci.*, 2023, **14**, 1966–1977.

2 T. W. Walker, N. Frelka, Z. Shen, A. K. Chew, J. Banick, S. Grey, M. S. Kim, J. A. Dumesic, R. C. Van Lehn and G. W. Huber, *Sci. Adv.*, 2020, **6**, 1–10.

3 K. L. Sánchez-Rivera, A. d. C. Munguía-López, P. Zhou, V. S. Cecon, J. Yu, K. Nelson, D. Miller, S. Grey, Z. Xu, E. Bar-Ziv, K. L. Vorst, G. W. Curtzwiler, R. C. Van Lehn, V. M. Zavala and G. W. Huber, *Resour., Conserv. Recycl.*, 2023, **197**, 107086.

4 V. Cappello, P. Sun, G. Zang, S. Kumar, R. Hackler, H. E. Delgado, A. Elgowainy, M. Delferro and T. Krause, *Green Chem.*, 2022, **24**, 6306–6318.

5 G. Celik, R. M. Kennedy, R. A. Hackler, M. Ferrandon, A. Tennakoon, S. Patnaik, A. M. LaPointe, S. C. Ammal, A. Heyden and F. A. Perras, *ACS Cent. Sci.*, 2019, **5**, 1795–1803.

6 *Nat. Nanotechnol.*, 2023, **18**, 687.

7 W. Zhang, H. Yao, R. Khare, P. Zhang, B. Yang, W. Hu, D. Ray, J. Hu, D. M. Camaioni, H. Wang, S. Kim, M. S. Lee, M. L. Sarazen, J. G. Chen and J. A. Lercher, *Angew. Chem.*, 2024, **136**, e202319580.

8 Y. Zhao, E. M. Rettner, K. L. Harry, Z. Hu, J. Miscall, N. A. Rorrer and G. M. Miyake, *Science*, 2023, **382**, 310–314.

9 J. M. Eagan, J. Xu, R. Di Girolamo, C. M. Thurber, C. W. Macosko, A. M. LaPointe, F. S. Bates and G. W. Coates, *Science*, 2017, **355**, 814–816.

10 S. D. Jaydev, A. J. Martin, D. Garcia, K. Chikri and J. Perez-Ramirez, *Nat. Chem. Eng.*, 2024, **1**, 565–575.

11 S. Crossley, J. Faria, M. Shen and D. E. Resasco, *Science*, 2010, **327**, 68–72.

12 F. Anaya and D. E. Resasco, *ACS Catal.*, 2020, **10**, 4433–4443.

13 D. Shi, J. Faria, T. N. Pham and D. E. Resasco, *ACS Catal.*, 2014, **4**, 1944–1952.

14 A. M. B. Rodriguez and B. P. Binks, *Soft Matter*, 2020, **16**, 10221–10243.

15 G. W. Huber and A. Corma, *Angew. Chem., Int. Ed.*, 2007, **46**, 7184–7201.

16 D.-P. Bui, L. A. Gomez, I. Alalq, L. Trevisi, A. C. Jerdy, H. K. Chau, L. L. Lobban and S. P. Crossley, *Catal. Sci. Technol.*, 2024, **14**, 4622–4630.

17 D.-P. Bui, L. A. Gomez, I. Alalq, L. Trevisi, A. C. Jerdy, H. K. Chau, L. L. Lobban and S. P. Crossley, *Catal. Sci. Technol.*, 2024, **14**, 4622–4630.

18 H. K. Chau, Q. P. Nguyen, A. C. Jerdy, D.-P. Bui, L. L. Lobban, B. Wang and S. P. Crossley, *ACS Catal.*, 2023, **13**, 1503–1512.

19 T. Omotoso, L. V. Herrera, T. Vann, N. M. Briggs, L. A. Gomez, L. Barrett, D. Jones, T. Pham, B. Wang and S. P. Crossley, *Appl. Catal., B*, 2019, **254**, 491–499.

20 S. Jongpatiwat, Z. R. Li, D. E. Resasco, W. E. Alvarez, E. L. Sughrue and G. W. Dodwell, *Appl. Catal., A*, 2004, **262**, 241–253.

21 N. M. Briggs, L. Barrett, E. C. Wegener, L. V. Herrera, L. A. Gomez, J. T. Miller and S. P. Crossley, *Nat. Commun.*, 2018, **9**, 3827.

22 D. W. Flaherty and E. Iglesia, *J. Am. Chem. Soc.*, 2013, **135**, 18586–18599.

23 Y. S. Yun, C. E. Berdugo-Díaz and D. W. Flaherty, *ACS Catal.*, 2021, **11**, 11193–11232.

24 T. O. Omotoso, B. Baek, L. C. Grabow and S. P. Crossley, *ChemCatChem*, 2017, **9**, 2642–2651.

25 H. Bahruji, M. Bowker, C. Brookes, P. R. Davies and I. Wawata, *Appl. Catal., A*, 2013, **454**, 66–73.

26 S. Kwon, T. C. Lin and E. Iglesia, *J. Catal.*, 2020, **383**, 60–76.

27 F. Huang, Z. Liu and Z. Yu, *Angew. Chem., Int. Ed.*, 2016, **55**, 862–875.

28 M. S. Ide, B. Hao, M. Neurock and R. J. Davis, *ACS Catal.*, 2012, **2**, 671–683.

29 J. Q. Bond, D. Martin Alonso, R. M. West and J. A. Dumesic, *Langmuir*, 2010, **26**, 16291–16298.

30 D. Spreitzer and J. Schenk, *Steel Res. Int.*, 2019, **90**, 1900108–1900125.

31 C. Xu, J. He, W. Zhang, H. Cui, J. Zhu and L. Hu, *ChemistrySelect*, 2020, **5**, 10081–10089.

32 M. B. Hugenschmidt, L. Gamble and C. T. Campbell, *Surf. Sci.*, 1994, **302**, 329–340.

33 J. Monnier, S. Réguer, E. Foy, D. Testemale, F. Mirambet, M. Saheb, P. Dillmann and I. Guillot, *Corros. Sci.*, 2014, **78**, 293–303.

34 M. Schettino Jr, J. Freitas, M. Morigaki, E. Nunes, A. Cunha, E. Passamani and F. Emmerich, *J. Nanopart. Res.*, 2010, **12**, 3097–3103.

35 K. D. Nixon, Z. O. G. Schyns, Y. Luo, M. G. Ierapetritou, D. G. Vlachos, L. T. J. Korley and T. H. III. Epps, *Nat. Chem. Eng.*, 2024, **1**, 615–626.

36 Low Density Polyethylene (LDPE) Price Trend and Forecast, https://www.chemanalyst.com/Pricing-data/low-density-polyethylene-ldpe-24, (accessed June 2024).

37 *Polymerscan*, S&P Global, 2023, https://www.spglobal.com/content/dam/spglobal/ci/en/documents/platts/en/products-services/market-reports/Polymerscan-010818.pdf.

38 K. L. Sanchez-Rivera, P. Zhou, M. S. Kim, L. D. Gonzalez Chavez, S. Grey, K. Nelson, S. C. Wang, I. Hermans, V. M. Zavala, R. C. Van Lehn and G. W. Huber, *ChemSusChem*, 2021, **14**, 4317–4329.

39 R. Feraldi, M. Huff, B. Sauer, S. Schneider, S. Cashman, A. Molen, J. Littlefield, W. Franklin, R. Hunt and L. Snook, *Cradle-to-gate life cycle inventory of nine plastic resins and four polyurethane precursors*, Franklin Associates, 2011.

40 Circular Packaging, https://www.creasolv.de/en/plants-projects/circular-packaging.html, (accessed January 2025).

41 G. Cabrera, J. Li, A. Maazouz and K. Lamnawar, *Polymers*, 2022, **14**, 2319.